Kinetic and Thermodynamic Study of Methyl Orange Dye Adsorption on Zinc Carbonyldiphthalate, an Organometallic-Based Material Prepared with a Montmorillonite Clay

Souad, Bennabi*+

Department of Chemistry, Faculty of Exact Sciences and Informatics, University of Hassiba Benbouali, B.P 78C, Ouled Fares, Chlef, ALGERIA

Nadir, Mahammed

Ecole Supérieure en Informatique 08 mai 1945, BP 73, El Wiam City, Sidi Bel Abbes, ALGERIA

ABSTRACT: *Our work is related to the use of adsorption as an effective physical method for water treatment contaminated with toxic dyes generated by various industries. We focused on the adsorption/removal of Methyl Orange (MO) dye from an aqueous solution using a new hybrid organometallic-based material constructed via In-Situ polymerization of Zinc-building units connected by coordination bonds to 4,4'-Carbonyldiphthalic acid (H_4CDPA) as a flexible multidentate organic ligand under solvothermal conditions with an amount of Maghnite-H^+, an acid-exchanged montmorillonite clay to obtain Zn-CDP/Mag-H^+ extremely stable thermally with an onset temperature of degradation upper to 460°C as shown by Thermogravimetric Analysis (TGA). The structure of this material is confirmed by Fourier Transform InfraRed (FT-IR) spectroscopy and X-Ray Diffraction (XRD). The effect of different parameters such as adsorbent mass, initial dye concentration, contact time, and pH of solution on the adsorption capacity of this material is investigated using UV-Visible spectroscopy. The kinetic study shows that the adsorption process of MO is very fast and well-described by the pseudo-second-order model. The adsorption isotherms of the adsorbent/adsorbate systems are in agreement with the Langmuir equation showing an adsorption capacity of 147.05 mg/g for this material. The thermodynamic parameters calculated at various temperatures indicate that MO adsorption on Zn-CDP/Mag-H^+ is an endothermic reaction ($\Delta H° > 0$) and spontaneous ($\Delta G° < 0$) process.*

KEYWORDS: *Organometallic material; Maghnite-H^+; Methyl Orange dye; Wastewater; Adsorption.*

* *To whom correspondence should be addressed.*
+ *E-mail: s.bennabi@univ-chlef.dz*
1021-9986/2023/1/123-138 16/$/6.06

INTRODUCTION

Environmental pollution is the result of population expansion becoming lately a major problem even if considerable efforts have been made in recent years to contain this phenomenon and eliminate pollutants. In particular, it is water pollution that has become the most challenging subject globally in the last few decades [1].

Dye wastewater has attracted considerable attention among all categories of polluted water. Many industries including paper, textiles, food, agrochemical applications and pharmaceutical production generate a considerable amount of wastewater contaminated by synthetic organic dyes and pigments [2].

Dyes can be ionic, aromatic organic compounds with structures including aryl rings, which have delocalized electron systems. The color of the dye is provided by their chromophore groups. They are everyday chemical compounds but highly visible, and undesirable and may have acute and/or chronic effects on living organisms depending on exposure time and concentration [3–5]. These pollutants are also endocrine disruptors interfering with the function of the natural hormones [6]. In addition, the release of dyes into surface waters also causes unwanted effects in the aquatic ecosystem [7].

The whole challenge for environmental scientists is to develop effective solutions for these hazardous pollutants. Furthermore, it is not easy to remove dye materials because of their degradation which is complicated by their high chemical and light stability [8]. Thus, several traditional approaches, whether physical, chemical, or biological, have been extensively used to achieve the tasks including flocculation [9] and coagulation [10] but with incomplete removal of the pollutants [11]. Sedimentation, filtration, reverse osmosis [12,13], extraction [14], and biological treatment [15] have also been used to eliminate these dyes but their application cannot be performed on a large scale because these methods usually require the use of sophisticated systems and the costs of operation are high [16,17].

Therefore, alternative approaches are necessary to replace the abovementioned conservative techniques. Adsorption technologies for complete removal of dyes have become more popular in recent years owing to their high efficiency on almost any type of dye or mixtures of dyes, sustainability, economic feasibility, and simplicity of design/operation as they can be carried out in mild conditions producing high quality water [18]. Physical adsorption is one of the most effective method for quickly lowering the concentration of dissolved dyes in an effluent using biomaterials, activated carbon, clay minerals, zeolites and industrial solid waste. However, the time required for the adsorption is slow with the difficulty of regenerating the used adsorbent [19].

Nonetheless, in the field of decomposition of organic pollutants, the photocatalytic degradation method is developed with the development of new materials based on inorganic nanoparticles non-toxic, and inexpensive. In fact, UV-Vis spectrophotometer reveals the photocatalytic performance of ZnO:SnO_2 for methyl orange and methylene blue degradation, which is enhanced with increasing the amount of SnO_2 nanoparticles in the hybrid material. Indeed, these nanoparticles prevent the fast recombination of produced surface charges, which results in an increase of MO oxidation [20,21]. The photocatalytic activity of decorated MWCNTs with ZnO nanoparticles is also investigated and showed that increasing the UV irradiation time and weight fraction led to the increase of the removal efficiency of MO dye thanks to the amount of photogenerated electron–hole pairs. Also, ZnO nanoparticles on the outer surface of MWCNTs are responsible for enhancing the photocatalytic activity of MWCNTs–ZnO hybrid by improving the active surface of this compound [22]. Nanocomposites like TiO_2–SnO_2 also shows significant removal efficiency of MO, which depends on the amount of SnO_2 nanoparticles on the outer surface of TiO_2 nanoparticles [23]. Another study on the synthesized MWCNTs@TiO_2 photocatalyst with TiO_2 nanoparticles reveals that this material can be used for the elimination of MO. Yet, the obtained results show that MWCNTs@TiO_2 exhibit a higher degradation rate of MO than that of TiO_2 nanoparticles [24].

Thanks to progress in materials design, there is also an emergence of a new generation of adsorbents known for their high surface areas and porosity. These materials are MOFs (Metal-Organic Frameworks), which represent relatively low-cost and efficient alternative adsorbents [25,26]. The structure of this new class of porous crystalline materials is composed of metal-oxide units (inorganic part) joined by organic ligands through strong covalent bonds. The metal-ligand interactions are stronger than hydrogen bonds, and have more directionality than other weak interactions, such as π-π stacking. While traditional

porous solids such as zeolites result from the interconnection of inorganic bricks with permanent characteristics, the large panel of used ligands and metal nodes allows the preparation of MOFs with different geometries, topologies, and pore sizes [27,28]. The flexibility of these materials can be modified giving ultra-high surface area, tunable pore size and volume, and adjustable internal surface properties, as well as high crystallinity and thermal stability [28]. These characteristics let them useful candidates for the treatment of wastewater due to the possibility of the presence of host–guest interactions through the chemical modification of the organic ligands and/or the inorganic sub-units [29,30]. According to Haque and coworkers, the protonated ethylenediamine-grafted Cr terephthalate (MIL-101) exhibits high adsorption capacity, rapid uptake and ready regeneration for the MO [31]. Iron terephthalate shows also a remarkable adsorption capacity of harmful dyes (anionic and cationic dyes) in the liquid phase, much higher than the commercially available activated carbon [32]. Even better, simultaneous adsorption of anionic and cationic dyes is achieved by MOF-235 even though it is considered a non-porous material since nitrogen is hardly adsorbed over the MOF-235 at low temperatures [32].

However, in some cases, the synthesis of these MOFs requires the use of toxic and dangerous catalysts such as hydrofluoric acid (HF) or nitric acid (HNO_3) [33,34], as well as the use of an autoclave which is not desirable from an industrial standpoint [32,35,36]. Moreover, most of the MOFs syntheses are carried out using slow-diffusion processes that take days or weeks to achieve, excluding the possibility of an industrially relevant process [37]. In this perspective, we investigate an alternative and efficient approach for the synthesis of a new organometallic-based material called Zn-CDP/Mag-H^+ inspired by MOFs' concept using an eco-catalyst called Maghnite-H^+ with the aim to respect the principles of green chemistry and also to improve the synthesis conditions (decreasing reaction time without using an autoclave). The structure of this material is characterized by Fourier Transform InfraRed (FT-IR) spectroscopy and X-Ray Diffraction (XRD). Its thermal stability is studied using ThermoGravimetric Analysis (TGA). The purpose of this work is also to examine the application of Zn-CDP/Mag-H^+ as a versatile and efficient material for the adsorption of Methyl Orange (MO) (Scheme 1). This dye has been selected, as it is inexpensive and widely

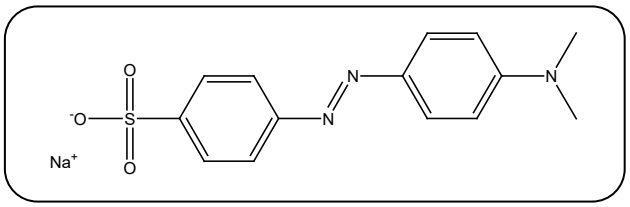

Scheme 1: Structure of Methyl Orange (MO) dye

used in textile, printing, paper, food, and pharmaceutical industries and research laboratories [38]. A kinetic and thermodynamic study of the adsorption phenomenon is also proposed by showing the effects of various operating parameters, such as adsorbent amount, contact time, initial dye concentration, and pH solution on the adsorption capacity of Zn-CDP/Mag-H^+.

EXPERIMENTAL SECTION

Materials

The Maghnite used in this work is provided from a quarry located in Maghnia (North West of Algeria) and supplied by the company "ENOF" (Algerian manufacturer specialized in the production of non-ferric products and useful substances). 4,4'-Carbonyldiphthalic acid (H_4CDPA) (98%, Aldrich), Zinc nitrate Hexa-hydrate ($Zn(NO_3)_2.6H_2O$) (98%, Aldrich), N,N-Dimethylformamide (C_3H_7NO) (99.8%, Aldrich), Sulfuric acid (H_2SO_4) (99.99%, Aldrich) and Chloroform ($CHCl_3$) (99.8%, Aldrich) are used as received without further purification. The dye Methyl orange having IUPAC name as Sodium 4-{[4-(dimethylamino)phenyl]diazenyl} benzene-1-sulfonate salt is obtained from Merck. All aqueous solutions are prepared with deionized and purified water.

Synthesis of Zn-CDP/Mag-H^+

In-situ polymerization of Zn-CDP/Mag-H^+ is carried out using a solvothermal method with N,N-dimethylformamide (DMF) as solvent (Fig. 1). An exact amount of 4,4'-Carbonyldiphthalic acid (H_4CDPA: 0.35 g, 1 mmol) is mixed with 50 mL of DMF. The mixture is stirred until the complete dissolution of the acid. Then, Zinc nitrate Hexa-hydrate ($Zn(NO_3)_2{\cdot}6H_2O$: 1.2 g, 4 mmol) and an amount of Maghnite-H^+ are added into the solution and stirred for few minutes at room temperature. The reactant mixture is kept in a closed vessel and heated at various times and temperatures to perform a kinetic study of this synthesis. A yellowish powder is collected by

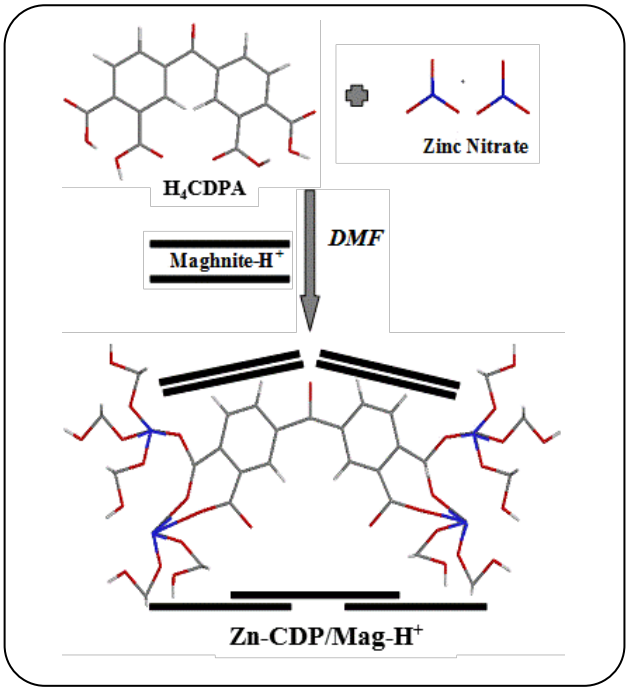

Fig. 1: Synthesis reaction of Zn-CDP/Mag-H⁺. Oxygen (red), Nitrogen (bleu), Carbon (grey).

filtration, repeatedly washed with fresh DMF, and dried at room temperature. The sample is stored in a vacuum desiccator to avoid water adsorption.

Adsorption tests

Zn-CDP/Mag-H$^+$ used for investigation of the dye adsorption is washed with chloroform (6 x 30 mL), then immersed in fresh chloroform (50 mL) for 48 h. After that, the product is filtered, dried and placed under vacuum at room temperature for 24 h, then kept in a desiccator. MO is dissolved in deionized water to prepare an aqueous stock solution of 200 mg/L. Aqueous solutions with different concentration of MO (10 – 50 mg/L) are prepared by successive dilution of the stock solution with water to obtain the calibration curve, which is plotted between absorbance and concentration of the dye solution to get absorbance-concentration profile. For adsorption kinetics and isotherm studies, the experiments are carried out in 100 mL sealed glass bottle containing an exact amount of the absorbent well mixed in the dye solution at room temperature by magnetic stirring and maintained for a fixed time. After the adsorption finished at time t, the solution is separated from the adsorbent by centrifugation (4000 rpm). The concentration of the residual dye is measured at a λ_{max} corresponding to the maximum adsorption for the dye solution (λ_{max} = 464 nm) after getting the UV spectra of the solution with the spectrophotometer. In order to determine the effect of aqueous solution pH on the adsorption of MO over Zn-CDP/Mag-H$^+$, the solution pH are adjusted in the range of 2-11 by adding a few drops of concentrated solutions of NaOH and HNO_3 0.1 M.

The dye concentration in the reaction mixture is calculated using the calibration curve. The equation is given by:

$$C_{MO} = (14.70 \times A_{464}) - 0.6955 \quad (1)$$

Where A_{464} is the absorbance of the sample at wavelength 464 nm.

The adsorption capacity q_t (mg/g) at time t (min) and the adsorption capacity q_e (mg/g) at equilibrium are calculated as follows:

$$q_t = \frac{(C_0 - C_t)\,V}{m} \quad (2)$$

$$q_e = \frac{(C_0 - C_e)\,V}{m} \quad (3)$$

Where C_0, C_t and C_e (mg/L) are the dye concentration at initial, any time t and at equilibrium in the solution, respectively. V (L) is the volume of the dye solution and m (g) is the mass of Zn-CDP/Mag-H$^+$.

Removal Efficiency (%) [39,40] is derived from the difference of the initial concentration and the final one:

$$RE\ \% = \frac{C_0 - C_t}{C_0} \times 100\% \quad (4)$$

Characterization methods

FT-IR experiments are recorded in the wavenumber range from 2000 to 400 cm^{-1}, on an Alpha Bruker FT-IR spectrometer based on Bruker Optics` patented RockSolid™ design, flexible sampling and Transmission, Attenuated Total Reflection (ATR), external and diffuse reflection FT-IR sampling accessories. The morphological characterization is carried out using Powder X-Ray Diffraction (PXRD) analysis conducted on a D8 DISCOVER Bruker diffractometer with The VÅNTEC-500 detector with Cu-Kα radiation (λ = 1.5418 Å). Thermogravimetric analyzes are recorded on a SETARAM Labsys TG-DTA/DSC (room temperature - 1600°C) with a nitrogen sweep of 200 mL/min. The temperature ramp is 10°C/min. The dye concentrations

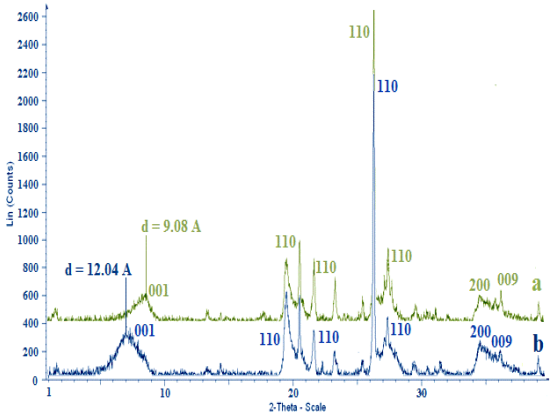

Fig. 2: X-Ray Diffraction of (a) Raw-Maghnite and (b) Maghnite-H+.

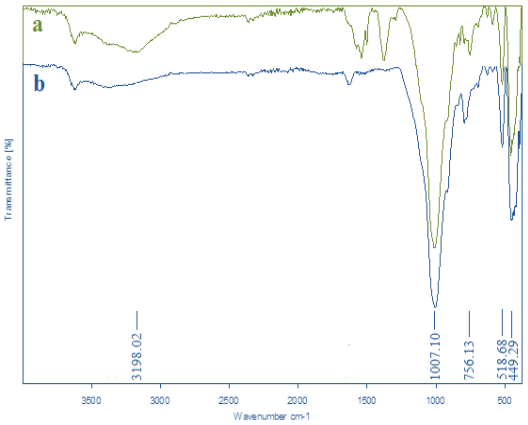

Fig. 3: FT-IR of (a) Raw-Maghnite and (b) Maghnite-H+.

in solution are measured by an Optizen 2120UV spectrophotometer and PH-2601 Bench pH Meter dual function is used to measure the pH values of the dye solutions.

RESULTS AND DISCUSSION

Characterization of Maghnite-H+

Maghnite-H^+ is a natural and non-toxic Montmorillonite-based catalyst with a lamellar structure, developed at the Polymer Chemistry Laboratory of the University of Oran, Alegria [41]. It shows remarkable catalytic capacities for polymerization reactions of several vinylic and heterocyclic monomers [42–47]. Maghnite-H^+ is prepared according to the reported method [47].

The morphological study by XRD reveals that the acid treatment of Maghnite leads to the substitution of interlamellar cations by H^+ protons, increasing the basal spacing from 9.08 Å in Raw-Maghnite (Fig. 2a), characteristic of a single water layer between the sheets, to a 12.04 Å, distance attributed to two interlamellar water layers in Maghnite-H^+ (Fig. 2b) [47]. FT-IR spectra (Fig. 3) [47] show bands at 3200 cm^{-1} for the characteristic absorption of the OH groups linked to the octahedral aluminum and at 1007 cm^{-1} for the Si-O stretching vibration in the tetrahedral layer. Angular deformation bands at 518 and 449 cm^{-1} are assigned to the type links of Si-O-M smectites, M may be Mg, Al or Fe. A low-intensity band at 750 cm^{-1} is assigned to the tetravalent silicon due to the presence of amorphous silica. XRD and FT-IR analysis state that Maghnite-H^+ is classified among the montmorillonite family according to the studies made by *M. Belbachir et al.* [41].

Kinetic studies of Zn-CDP/Mag-H+ synthesis

Kinetic studies (Fig. 4) show that the highest yields of Zn-CDP/Mag-H^+ are obtained with an amount of 20% by weight of Maghnite-H^+, for a reaction time and temperature of 28 hours and 110°C, respectively. Zn-CDP/Mag-H^+ (20 wt % of Maghnite-H^+) will be used for all experiments performed in this work.

Structure determination of Zn-CDP/Mag-H+

FT-IR spectra of Zn-CDP/Mag-H^+ (Fig. 5b) show the disappearance of the intense and large characteristic bands of OH group (3210 cm^{-1} and 927 cm^{-1}) confirming the complete deprotonation of 4,4'-Carbonyldiphthalic acid. The sharp bands at 1549 cm^{-1} and at 1375 cm^{-1} are ascribed to the symmetric and asymmetric motions of the COO^- carboxylate group. The band at 680 cm^{-1} corresponds to the Zn-O stretching vibration. There are also the usual characteristic frequencies of Maghnite-H^+, a broad band at 1032 cm^{-1} for the Si-O vibration and deformation bands at 515 cm^{-1} and 459 cm^{-1} corresponding to Si-O-Al group. Finally, the elongation vibration at 1491 cm^{-1} attributed to the aromatic group C=C (Fig. 5b) is involved in the adsorption mechanism via π-π interactions between MO molecules and Zn-CDP/Mag-H^+ as will be stated in the following sections.

XRD analysis of Zn-CDP/Mag-H^+ (Fig. 6) shows a broad peak in the region of small angles, confirming the presence of Maghnite-H^+ in the structure of this material. The sharp and intense peak at $2\theta = 9.9°$ confirms the high crystallinity and ordered structure of Zn-CDP/Mag-H^+ and that the final layout of this material is not altered by Maghnite-H^+. There is an increaseinf the interlayer space

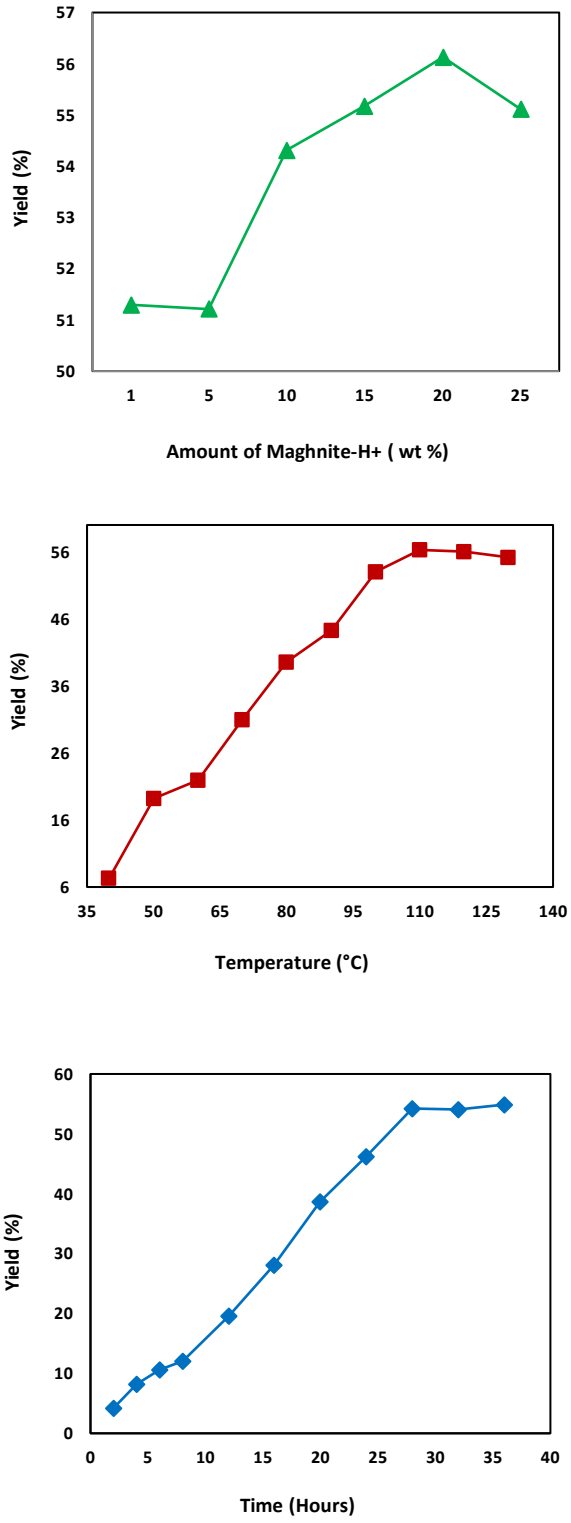

Fig. 4: Effect of the amount of Maghnite-H$^+$, temperature, and time on the yield of Zn-CDP/Mag-H$^+$.

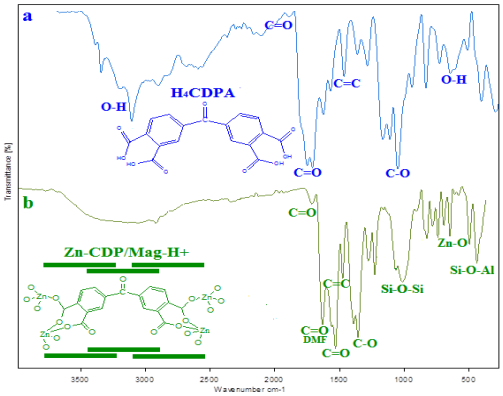

Fig. 5: FT-IR spectra of (a) H_4CDPA and (b) Zn-CDP/Mag-H$^+$.

d_{001} from 12.04 Å for Maghnite-H$^+$ alone to 13.77 Å for Zn-CDP/Mag-H$^+$ (Fig. 7) resulting from the intercalation of some Zn-CDP chains between the sheets of the clay. The correlation peak of Maghnite-H$^+$ is much less intense than that of Zn-CDP/Mag-H$^+$, the latter exhibits a more orderly crystalline stacking of the sheets compared to the clay.

Thermogravimetric analysis of Zn-CDP/Mag-H$^+$ (Fig. 8) shows that this material is thermally very stable with an onset temperature of degradation extraordinarily high (469°C). TGA curve of this material shows three main steps of weight loss. The first mass loss (11.03%) between 86°C and 146°C is attributed to the dehydration process (removal of physically adsorbed water molecules on the surface of Zn-CDP/Mag-H$^+$). The second mass loss (14.41%) between 316°C and 358°C may be associated with the removal of DMF molecules trapped in the material pores; and also some residual molecules of the acid (H_4CDPA) that have not reacted. The final step and the prominent weight loss (33.16%) around 542°C is related to the collapse and degradation of the Zn-CDP/Mag-H$^+$ structure. There is a total mass loss of 58% when the temperature reaches 542°C. The residual amount maybe the conversion of the material into ZnO_2.

Adsorption studies

Effect of adsorbent amount

Different amounts of Zn-CDP/Mag-H$^+$ are mixed with 50 mL of MO solution at a concentration of 50 mg/L for 10 minutes. A mass of 30 mg of Zn-CDP/Mag-H$^+$ fixes a maximum dye (Fig. 9). From this mass, the percentage

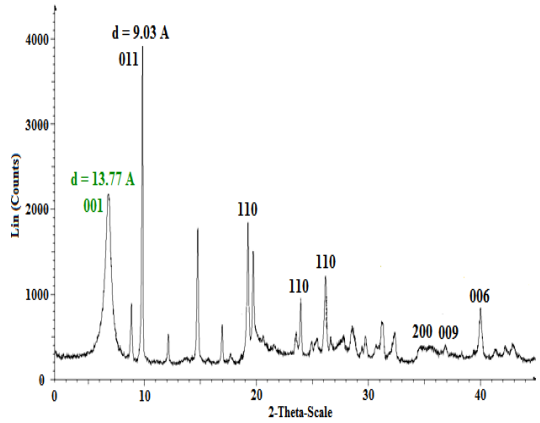

Fig. 6: XRD pattern of Zn-CDP/Mag-H$^+$.

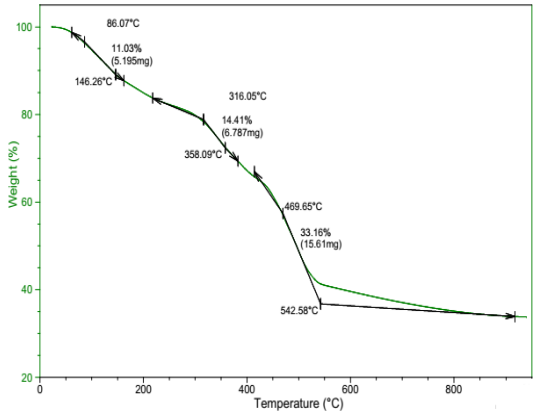

Fig. 8: Thermogram TGA of Zn-CDP/Mag-H$^+$.

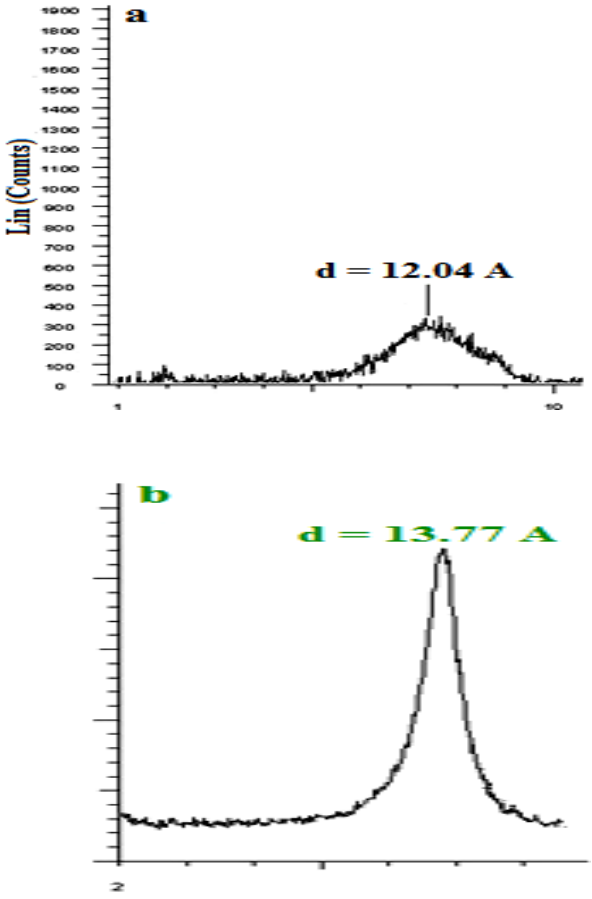

Fig. 7: XRD patterns of: (a) Maghnite-H$^+$ and (b) Zn-CDP/Mag-H$^+$.

of removed dye reaches equilibrium. Also, the amount of the adsorbed dye increases in the beginning but decreases as the dosage of adsorbent increases from 30 mg to 50 mg.

In fact, increasing the adsorbent amount rises the total surface area making available a very large number of adsorption sites until the mass 30 mg from which there is an overlapping or aggregation of adsorption sites, consequently, a reduction in the total adsorption surface area with a decrease in the amount of adsorbate per unit mass of adsorbent. Thus, a relatively high dosage of the adsorbent leads to a high adsorption rate but a low adsorption quantity. For theses results, it is necessary to avoid ineffective overdose. In the rest of the work and to determine the adsorption capacities by saturating all the probable sites, we chose to work with adsorbent mass of 30 mg.

Effect of initial dye concentration as a function of time

The initial dye concentration and contact time are crucial factors influencing the adsorption capacity of an adsorbent in wastewater treatment systems. The evolution curves (Fig. 10a) show that MO interacts with Zn-CDP/Mag-H$^+$ rapidly during the first 40 minutes, then the adsorption slows down and approaches equilibrium in nearly 110 min where the maximum adsorption of MO onto Zn-CDP/Mag-H$^+$ is observed. This equilibrium is the result of the saturation of the adsorption sites in this material by the dye. Based on these results, 110 minutes is taken as the equilibrium time in batch adsorption experiments on this material. This phenomenon is comparable for all three concentrations.

Furthermore, the amount of adsorbed dye increases with the initial dye concentration showing the favorable adsorption at high dye concentration. Indeed, the mass

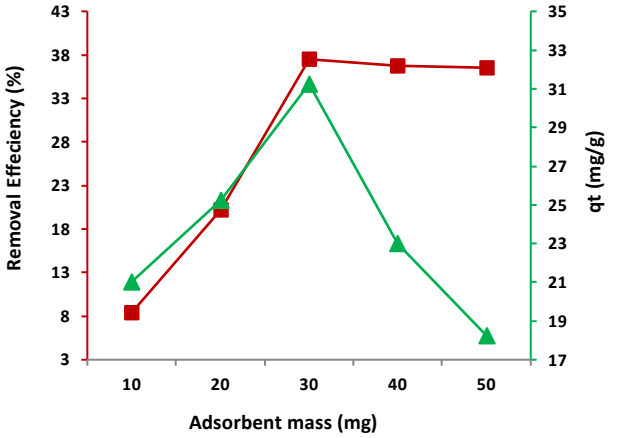

Fig. 9: Effect of Zn-CDP/Mag-H$^+$ mass on percentage and amount of MO removal (C_0 = 50 mg/L, V = 50 mL, pH = neutral, contact time = 10 min).

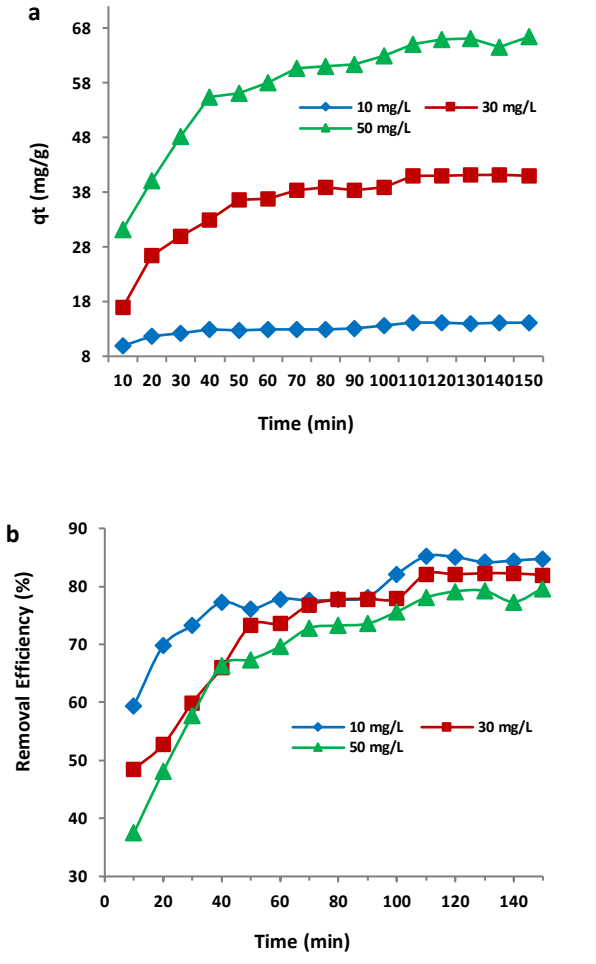

Fig. 10: (a,b) Effect of contact time and initial dye concentration on the adsorption of MO on Zn-CDP/Mag-H$^+$ (V = 50 mL, $m_{adsorbent}$ = 30 mg, pH = neutral).

the gradient between the solution and adsorbent increases with the increase of the initial dye concentration, accelerating the transfer of dye molecules from the bulk solution to the particle surface due to the increase in the driving force of the concentration gradient. However, the removal rate of MO on Zn-CDP/Mag-H$^+$ is higher at the lower initial concentration (Fig. 10b).

Effect of pH values

The pH solution is an important parameter since the adsorption capacity of the dye strongly depends on it, which is attributed to the ratio of H^+/OH^- in aqueous solution that affects the structure of the dye as well as the surface charges of the adsorbent [48]. The effect of initial pH on MO adsorption toward Zn-CDP/Mag-H$^+$ is investigated in the pH range from 2 to 11 (Fig. 11). The experiments are carried out by adding 30 mg of the adsorbent to 50 mL of the dye solution with an initial concentration of 50 mg/L at 298 K for a contact time of 110 min (equilibrium time in this work). The adsorption mechanisms may be attributed to electrostatic interactions between the dye and the adsorbent. In fact, from the Point of Zero Charge of Zn-CDP/Mag-H$^+$ (pH_{PZC} = 6 to 9), the surface charge is positive for solutions with a pH < pH_{PZC}, providing good adsorption and selective separation ability for this adsorbent towards the anionic dyes. Therefore, there will be a strong electrostatic attraction with MO molecules that are converted to anionic form above pH of 3.47 (pKa value of MO is 3.47 [49]), which explains the highest adsorption capacity that increases at pH value between 3 and 6. These results are quite similar to previously reported results [34, 36]. However, there is a decrease of the adsorption capacity at higher pH values (pH > pH_{PZC}) indicating that the surface charge of Zn-CDP/Mag-H$^+$ becomes more negative, increasing the electrostatic repulsions of MO anions. Nevertheless, it is noticed that the adsorption capacity is around 25 mg/g even when MO molecules are neutral showing that there are possible other mechanisms controlling the adsorption capacity like π-π interactions between the benzene rings of MO and the benzene rings in Zn-CDP/Mag-H$^+$ [50,51]

Adsorption kinetics

Pseudo-first-order and pseudo-second-order [52] are two kinetic models used to investigate the adsorption behaviors and mechanism of MO sorption on

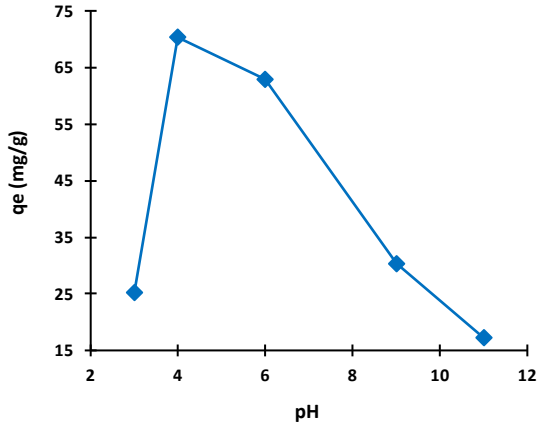

Fig. 11: Effect of initial pH on the adsorption of MO over Zn-CDP/Mag-H⁺ (C_0 = 50 mg/L, V = 50 mL, $m_{adsorbent}$ = 30 mg, contact time = 110 min).

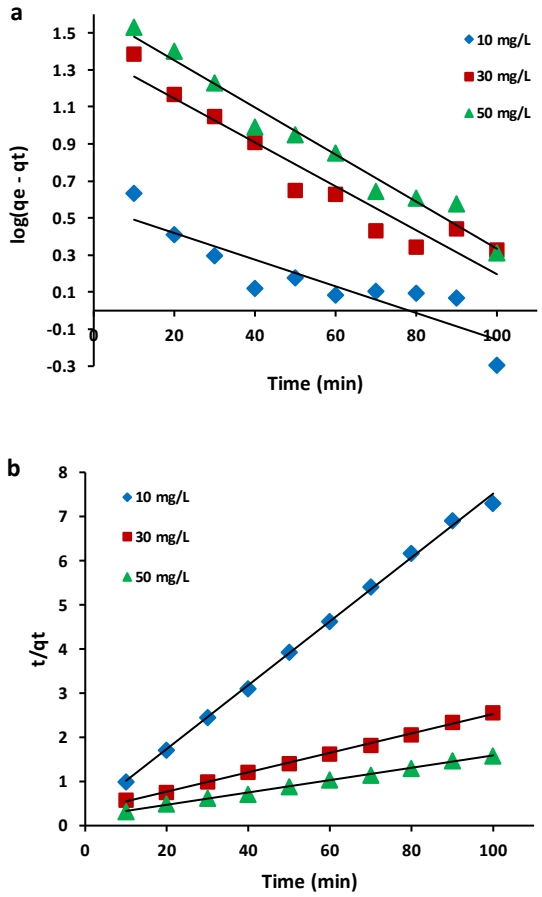

Fig. 12: Linear regressions of MO according to (a) pseudo-first-order kinetic model and to (b) pseudo-second-order kinetic model at different initial dye concentrations (V = 50 mL, $m_{adsorbent}$ = 30 mg, pH = neutral).

Zn-CDP/Mag-H⁺ at the three initial dye concentrations (10 mg/L, 30 mg/L, 50 mg/L) and at fixed adsorbent amount (30 mg). The two rate expressions based on the adsorption capacity are expressed as follows:

Pseudo-first-order:

$$\log(q_e - q_t) = \log q_e - \frac{k_1}{2.303}t \quad (5)$$

Pseudo-second-order:

$$\frac{t}{q_t} = \frac{1}{k_2 q_e^2} + \frac{1}{q_e}t \quad (6)$$

Where q_e and q_t (mg/g) represent the amount of the adsorbed dye per Zn-CDP/Mag-H⁺ unit at equilibrium and at any time t, respectively. k_1 (min^{-1}) named the Lagergren rate constant of adsorption is obtained from the slope of the linear regression of the above-mentioned equation (Fig.12), and k_2 (g/mg.min) is the pseudo-second-order rate.

The obtained data shown in Table 1 fit with poor correlation coefficient R^2 values (0.802 to 0.973) at different initial dye concentrations indicating that the adsorption mechanism does not follow the pseudo-first-order model. In addition, the calculation of q_e for the three concentrations shows that the amounts of adsorbed dye are small compared to the experimental amounts. These observations demonstrate that the MO adsorption does not express a process of controlled diffusion. The adsorption data analyzed using the pseudo-second-order model show that the correlation coefficient values are very close to 1 (R^2 > 0.99) indicating that this model is suitable for MO adsorption on Zn-CDP/Mag-H⁺. In addition, q_e values are almost equivalent to that calculated. From Table 1, the calculated kinetic constant k_2 decreases with increasing initial dye concentration indicating slow adsorption when the concentration of initial dye increases as can be seen previously (Fig. 10) where the amount of adsorbed dye reaches its equilibrium more quickly for low dye concentrations. This phenomenon is owing to the weaker competition of the adsorption surface sites at lower concentrations [53], similar results are obtained for other MOFs [54–57].

Adsorption isotherms

Adsorption isotherms are used to further describe the adsorption progress by determining the maximum adsorption capacity of MO on Zn-CDP/Mag-H⁺ and

Table 1: Kinetic parameters for MO adsorption over Zn-CDP/Mag-H$^+$ at different concentrations of MO.

C_0 (mg/L)	$q_{e,exp}$ (mg/g)	Pseudo-first-order			Pseudo-second-order		
		$q_{e,cal}$ (mg/g)	k_1 (min^{-1})	R^2	$q_{e,cal}$ (mg/g)	k_2 (g/mg.min)	R^2
10	14.18	3.64	1.612 x 10^{-2}	0.802	13.88	1.775 x 10^{-2}	0.998
30	41.04	24.09	2.533 x 10^{-2}	0.925	45.45	1.471 x 10^{-3}	0.997
50	65.05	40.27	2.763 x 10^{-2}	0.973	71.42	1.020 x 10^{-3}	0.998

to identify the adsorption mechanism by describing the interactive behavior between adsorbate and adsorbent. The experimental data process according to the mathematical models of Langmuir and Freundlich:

The Langmuir equation [58]:

$$\frac{C_e}{q_e} = \frac{1}{QK_L} + \frac{C_e}{Q} \quad (7)$$

Where C_e (mg/L) is the equilibrium concentration of the adsorbate, Q (mg/g) is the maximum adsorption capacity, and K_L (L/mg) is the Langmuir constant related to the equilibrium of adsorption.

The dimensionless separation factor R_L can be presented as follows [59]:

$$R_L = \frac{1}{1 + (K_L C_0)} \quad (8)$$

Where C_0 is the initial concentration of MO (mg/L). The model is suggested to be favorable if $0 < R_L < 1$.

The Freundlich equation [60]:

$$\log q_e = \log K_F + \frac{1}{n} \log C_e \quad (9)$$

Where K_F (mg/g)(L/mg)$^{1/n}$ is the Freundlich constant related to the adsorption capacity of the adsorbent and n indicate the degree when an adsorption process is favorable. A value of $\frac{1}{n}$ between 0 and 1 indicates favorable adsorption.

The Langmuir model presumes that the adsorption is reversible with a monolayer of adsorbate molecules formed homogeneously on the adsorbent surface. It means that the adsorption occurs at a fixed number of specific and equivalent energy sites. Each site can adsorb only one dye molecule with the decrease of interaction forces between adsorbed molecules, even on adjacent sites [61]. Then, a saturation value is reached and no other type of adsorption can take place in this site. The Freundlich isotherm model describes the adsorption capacity associated to the dye concentration at equilibrium and assumes that the adsorption occurs on a heterogeneous surface corresponding to a multi-site adsorption isotherm involving different sites with several adsorption energies [62].

Equilibrium adsorption isotherms are conducted at different concentrations ranging from 10 to 50 mg/L with a fixed adsorbent mass (30 mg) and contact time (110 min). After determining the residual concentrations of the supernatants, first, we plot (C_e/q_e) vs C_e according to Langmuir's model and secondly, $log\ q_e$ vs $log\ C_e$ according to Freundlich's model (Fig.13).

The obtained results reported in Table 2 show that the adsorption of MO onto Zn-CDP/Mag-H$^+$ fits Langmuir model better than Freundlich model based on R^2 values. The good correlation between the adsorption data and the Langmuir model confirms the homogeneous distribution of active sites on the adsorbent in monolayer coverage of dye molecules. The favorability of the adsorption system can be further anticipated. In fact, the calculated dimensionless separation factor R_L which are ranging between 0 and 1 ($0.217 \leq R_L \leq 0.581$), indicate the favorable uptake of the MO process. The obtained n value from the Freundlich model is greater than unity ($n = 1.308$) illustrating that the adsorption intensity is good and favorable at high concentrations but much less at lower concentrations. K_F value also shows that Zn-CDP/Mag-H$^+$ has a very high adsorption capacity for MO in aqueous solutions.

The maximum uptake capacity of the composite is Q = 147.05 mg/g. This result is compared with the adsorption capacity of different MOFs toward MO reported previously. As it is noticed from Table 3, the adsorption capacity value of Zn-CDP/Mag-H$^+$ is not the highest. However, this material can be considered as a good and suitable adsorbent for anionic dyes such as MO.

Table 2: Langmuir and Freundlich parameters for MO adsorption over Zn-CDP/Mag-H$^+$.

Langmuir isotherm			Freundlich isotherm		
Q (mg/g)	K_L (L/mg)	R^2	K_F (mg/g)(L/mg)$^{1/n}$	n	R^2
147.05	0.072	0.999	10.889	1.308	0.9951

Table 3: The adsorption capacity of various MOFs toward MO.

MOF	Experimental conditions	Adsorption capacity	Reference
MIL-100 (Cr)	C_0: 1000 mg/L t = 3 days	211.8 mg/g	[33]
MOF-235	C_0: 20-200 mg/L t = 12 h	477 mg/g	[32]
ZIF-11	C_0: 800 mg/L t = 40 min	178.57 mg/g	[64]
MIL-101	C_0: 30-50 mg/L t = 12 h	114 mg/g	[34]
PED-MIL-101	C_0: 30-50 mg/L t = 12 h	194 mg/g	[34]
NH2-MIL-101(Al)	C_0: 40 mg/g t = 12 h	188 mg/g	[35]
UiO-66-NH_2	C_0: 80 mg/g t = 180 min	83.7 mg/g	[63]
Zn-CDP/Mag-H$^+$	C_0: 10-50 mg/L t = 110 min	147.05 mg/g	This work

MIL stands for Material of Institute Lavoisier
UiO stands for University of Oslo
ZIF stands for Zeolitic Imidazolate Framework

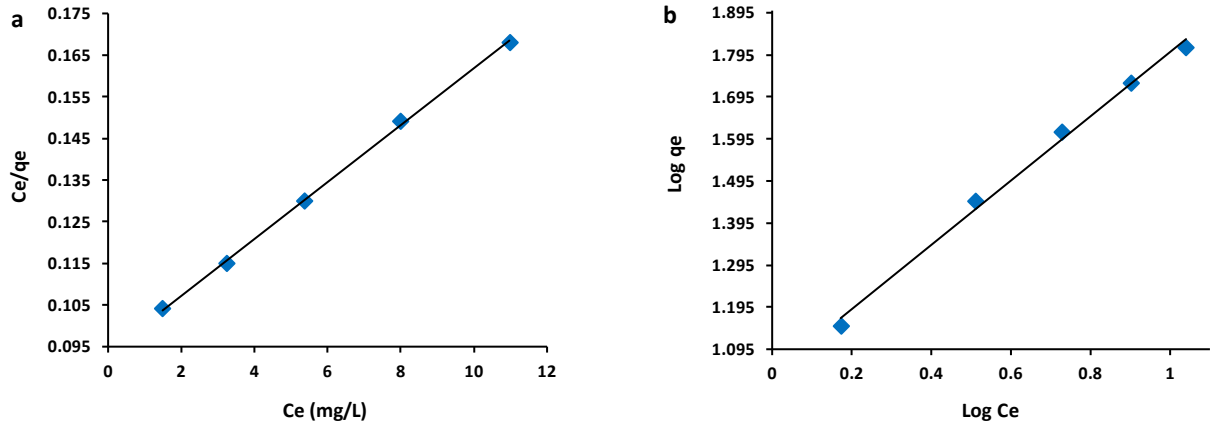

Fig. 13: Adsorption isotherm models for MO dye adsorption over Zn-CDP/Mag-H$^+$: (a) Langmuir isotherm, (b) Freundlich isotherm (V = 50 mL, $m_{adsorbent}$ = 30 mg, pH = neutral, contact time = 110 min).

Thermodynamic studies

Adsorption is a phenomenon that can be exothermic or endothermic depending on the adsorbent material and the nature of the adsorbed molecules [65]. Thus, the adsorption thermodynamic parameters are used to further investigate spontaneity and mechanism of MO adsorption onto Zn-CDP/Mag-H$^+$. The temperature effect is studied in the range 298 – 333 K. The changes in adsorption enthalpy ($\Delta H°$), entropy ($\Delta S°$) and Gibbs free energy ($\Delta G°$) are calculated and listed in Table 3 from the following equations [66,67]:

$$\Delta G^\circ = -RT \ln K_0 \quad (10)$$

$$K_0 = \frac{q_e}{Ce} \quad (11)$$

$\Delta H°$ and $\Delta S°$ can be obtained from the Van't Hoff equation:

$$\ln K_0 = \frac{\Delta S^\circ}{R} - \frac{\Delta H^\circ}{RT} \quad (12)$$

Table 4: Thermodynamic parameters of MO adsorption over Zn-CDP/Mag-H$^+$ at different temperatures.

Temperature (K)	K_0 (L/g)	ΔG° (kJ/mol)	ΔH° (kJ/mol)	ΔS° (J/mol K)
298	5.92	-4.405		
313	6.80	-4.983	7.43	39.68
333	8.10	-5.789		

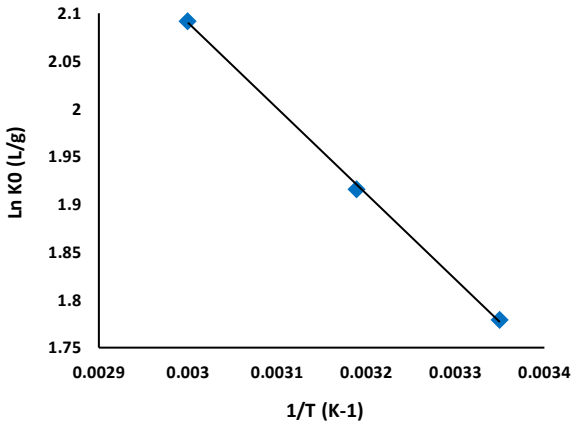

Fig. 14: Van't Hoff plot to get ΔH° and ΔS° of MO adsorption over Zn-CDP/Mag-H$^+$ (C_0 = 50 mg/L, V = 50 mL, $m_{adsorbent}$ = 30 mg, pH = neutral, contact time = 100 min).

Where K_0 is the thermodynamic equilibrium constant, T is the temperature (K), and R is the gas constant (8.314 J/mol K). The values of $\Delta H°$ (KJ/mol) and $\Delta S°$ (J/mol.K) are obtained from the slope and intercept of a linear plot between $Ln\ K_0$ and 1/T (Fig. 14).

The $\Delta G°$ values are all negative for different temperatures suggesting that the adsorption of MO on Zn-CDP/Mag-H$^+$ is spontaneous and feasible under the experimental conditions with a slight increase in the degree of spontaneity of the reaction when the temperature increases. This can be explained by the decrease in the thickness of the boundary layer surrounding the adsorbent with temperature, improving the mass transfer of the adsorbate from the solution [68]. Furthermore, these results indicate that the adsorption process is physisorption (-20 kJ/mol < $\Delta G°$ < 40 kJ/mol) rather than chemisorption (-80 kJ/mol < $\Delta G°$ < -400 kJ/mol) [69].

The data shown in Table 4 indicate that the calculated $\Delta H°$ value is positive confirming the endothermic behavior of the adsorption process corresponding to the increasing adsorption capacity related to the increasing temperature. The interactions between pre-adsorbed water and the adsorbent are stronger than that the interaction between MO and Zn-CDP/Mag-H$^+$, which explain the endothermic adsorption [32]. The positive value of $\Delta S°$ indicates an increase of the randomness at the solid-solution interface during adsorption and the affinity of the adsorbent for the dye possibly because the number of desorbed water molecule is larger than that of the adsorbed MO molecules since dyes are more bulky than water leading to the desorption of several water molecules when dye molecules are adsorbed [54]. This positive value also reflects that no critical change occurs in the internal structure of the solid during adsorption of the dye. As a consequence, the adsorption process would be controlled by an entropy effect (positive S) rather than an enthalpy change (positive H).

CONCLUSIONS

In summary, a new hybrid material Zn-CDP/Mag-H$^+$ is successfully synthesized using Maghnite-H$^+$, an acid-exchanged montmorillonite clay. FT-IR spectroscopy confirms the structure of this material and XRD patterns show that it has a crystalline and ordered arrangement. TGA shows that this material is thermally stable with a high temperature of degradation (469°C). The experimental results show also that Zn-CDP/Mag-H$^+$ exhibits a rapid and an efficient adsorption towards MO in aqueous solution with an adsorption capacity reaching 147.05 mg/g. The adsorption process reveals that the amount of adsorbed dye per gram of Zn-CDP/Mag-H$^+$ increases with increasing initial dye concentration in the solution and the optimum amount of adsorbent is 30 mg. The kinetic study of MO adsorption on Zn-CDP/Mag-H$^+$ is controlled by the pseudo-second-order model showing that the adsorption process is very fast during the first 40 minutes, with a maximum uptake of dye reached at 110 minutes. Adsorption of MO at various pH values suggests that adsorption mechanisms mainly involve electrostatic interactions between the dye and Zn-CDP/Mag-H$^+$ as well as π-π stacking between the benzene rings of MO and the benzene rings of the material. It is noticed that the adsorption isotherms are well described by the Langmuir equation which represents the best fit of experimental data. The calculated thermodynamics parameters at various temperature ($\Delta G° < 0$, $\Delta H° > 0$ and $\Delta S° > 0$) suggest that the adsorption of MO on Zn-CDP/Mag-H$^+$ is spontaneous and endothermic

and the driving force of the adsorption is controlled by an entropy effect rather than an enthalpy change. The results of this study clearly demonstrate that Zn-CDP/Mag-H^+, an organometallic-based material, has considerable potential as a promising adsorbent in wastewater treatment for the adsorptive-removal of toxic dyes. Specific applications as well as reuse and recovery of this material may be of further scope of research.

Acknowledgments

This work has no financial support. The authors declare that they have no conflict of interest. The authors would like to especially thank Zakaria Cherifi, PhD degree in Green Chemistry (Laboratory of Polymer Chemistry, the University of Oran1 Ahmed BenBella, Algeria) for FT-IR and XRD analysis.

Received : Dec. 8, 2021 ; Accepted : Feb. 14, 2022

REFERENCES

[1] Wong J.K.H., Tan H.K, Lau S.Y., Yap P.S., Danquah M.K., Potential and Challenges of Enzyme Incorporated Nanotechnology in Dye Wastewater Treatment: A Review, *J. Environ. Chem. Eng.,* **7(4)**: 103261-103278 (2019).

[2] Benkhaya S., M'rabet S., El Harfi A., A Review on Classifications, Recent Synthesis and Applications of Textile Dyes, *Inorg. Chem. Commun.* **115**: 107891-107926 (2020).

[3] Hsieh H.Y., Huang K.C., Cheng J.O., Lo W.T., Meng P.J., Ko F.C., Environmental Effects on the Bioaccumulation of PAHs in Marine Zooplankton in Gaoping Coastal Waters, Taiwan: Concentration, Distribution, Profile, And Sources, *Mar. Pollut. Bull.,* **144**: 68-78 (2019).

[4] Lellis B., Fávaro-Polonio C.Z., Pamphile J.A., Polonio J.C., Effects of Textile Dyes on Health and the Environment and Bioremediation Potential of Living Organisms, *Biotechnol. Res. Innov.,* **3(2)**: 275-290 (2019).

[5] Ren X., Zeng G., Tang L., Wang J., Wan J., Liu Y., Yu J., Yi H., Ye S., Deng R., Sorption, Transport and Biodegradation – An Insight Into Bioavailability of Persistent Organic Pollutants in Soil, *Sci. Total Environ.,* **610**: 1154-1163 (2018).

[6] Jun B.M., Hwang H.S., Heo J., Han J., Jang M., Sohn J., Park C.M., Yoon Y., Removal of Selected Endocrine-Disrupting Compounds Using Al-Based Metal Organic Framework: Performance and Mechanism of Competitive Adsorption, *J. Ind. Eng. Chem.,* **79**: 345-352 (2019).

[7] Mashkoor F., Nasar A., Inamuddin, Asiri A.M., Exploring the Reusability of Synthetically Contaminated Wastewater Containing Crystal Violet Dye using Tectona grandis Sawdust as a Very Low-Cost Adsorbent, *Sci. Rep.,* **8**: 8314- 8330 (2018).

[8] Collivignarelli M.C, Abbà A., Carnevale Miino M., Damiani S., Treatments for Color Removal from Wastewater: State of the Art, *J. Environ. Manag.,* **236**: 727-745 (2019).

[9] Melo R.P.F., Carmo S.K.S., Barros E.L.B., Câmara A.G., Nunes S.K.S., Barros Neto E.L., Removal of Disperse Blue 56 from Synthetic Textile Effluent Using Ionic Flocculation, *Water Sci Technol,* **83(11)**: 2714-2723 (2021).

[10] Jargalsaikhan M., Lee J., Jang A., Jeong S., Efficient Removal of Azo Dye from Wastewater Using the Non-Toxic Potassium Ferrate Oxidation–Coagulation Process, *Appl. Sci.,* **11(15)**: 6825- 6836 (2021).

[11] Pavithra K.G, Kumar P.S., Jaikumar V., Rajan P.S., Removal of Colorants from Wastewater: A Review on Sources and Treatment Strategies, *J. Ind. Eng. Chem.,* **75**: 1-19 (2019).

[12] Gupta B, Priya T., Kumar Mishra B., Augmentation of the Coagulation Activity of Alum Using a Porous Bio-Flocculant for the Remediation of Trihalomethanes-Generating Hydrophobic Natural Organic Matter, *Environ. Eng. Res.,* **26(3)**: 209-217 (2020).

[13] Pronk W., Ding A., Morgenroth E., Derlon N., Desmond P., Gravity-Driven Membrane Filtration for Water and Wastewater Treatment: A Review, *Water Res.,* **149**: 553-565 (2019).

[14] Bukman L., De Souza V.R., Fernandes N.R.C., Caetano W., Batistela V.R., Hioka N., Reverse Micellar Extraction of Dyes Based on Fatty Acids and Recoverable Organic Solvents, *Sep. Purif. Technol.,* **242**: 116772- 116780 (2020).

[15] Dassanayake R.S, Acharya S., Abidi N., Recent Advances in Biopolymer-Based Dye Removal Technologies, *Molecules,* **26(15)**: 4697- 4717 (2021).

[16] Zeneli A., Kastanaki E., Simantiraki F., Gidarakos E., Monitoring the Biodegradation of TPH and PAHs in Refinery Solid Waste by Biostimulation and Bioaugmentation, *J. Environ. Chem. Eng.,* **7(3)**: 103054- 103061 (2019).

[17] Gaur N., Narasimhulu K., PydiSetty Y., Recent Advances in the Bio-Remediation of Persistent Organic Pollutants and its Effect on Environment, *J. Clean. Prod.,* **198**: 1602-1631 (2018).

[18] Dutta S., Srivastava S.K., Gupta B., Gupta A.K., Hollow Polyaniline Microsphere/MnO_2/Fe_3O_4 Nanocomposites in Adsorptive Removal of Toxic Dyes from Contaminated Water, *Mater. Adv.,* **13(45)**: 54324–54338 (2021).

[19] Szczęśniak B., Phuriragpitikhon J., Choma J., Jaroniec M., Recent Advances in the Development and Applications of Biomass-Derived Carbons with Uniform Porosity, *J. Mater. Chem. A,* **8(36)**: 18464-18491 (2020).

[20] Ghaderi A., Abbasi S., Farahbod F., Synthesis, Characterization and Photocatalytic Performance of Modified ZnO Nanoparticles with SnO_2 Nanoparticles, *Mater. Res. Express*., **5(6)**: 065908-065919 (2018).

[21] Abbasi S., Ekrami-Kakhki M.-S., Tahari M., Modeling and Predicting the Photodecomposition of Methylene Blue via ZnO–SnO_2 Hybrids Using Design of Experiments (DOE), *J. Mater. Sci.: Mater. Electron.*, **28(3)**: 15306–15312 (2017).

[22] Roozban N., Abbasi S., Ghazizadeh M., Statistical Analysis of the Photocatalytic Activity of Decorated Multi-Walled Carbon Nanotubes with ZnO Nanoparticles, *J. Mater. Sci.: Mater. Electron.*, **28(8):** 6047–6055 (2017).

[23] Abbasi S., Hasanpour M., Ahmadpoorb F., Sillanpää M., Dastan D., Achour A., Application of the Statistical Analysis Methodology for Photodegradation of Methyl Orange Using a New Nanocomposite Containing Modified TiO_2 Semiconductor with SnO_2, *Int. J. Environ. Anal. Chem*., **101(2)**: 208-224 (2021).

[24] Abbasi S., The Degradation Rate Study of Methyl Orange Using MWCNTs@TiO_2 as Photocatalyst, Application of Statistical Analysis Based on Fisher's F Distribution, *J. Clust. Sci.*, 1-10 (2021).

[25] Khan M.S., Khalid M., Ahmad M.S., Shahid M., Ahmad M., Catalytic Activity of Mn(III) and Co(III) Complexes: Evaluation of Catechol Oxidase Enzymatic and Photodegradation Properties, *Res. Chem. Intermed.,* **46**: 2985-3006 (2020).

[26] Xiang W., Zhang Y., Chen Y., Liu C.J, Tu X., Synthesis, Characterization and Application of Defective Metal–Organic Frameworks: Current Status and Perspectives, *J. Mater. Chem. A,* **8**: 21526- 21546 (2020).

[27] Begum S., Hassan Z., Bräse S., Tsotsalas M., Polymerization in MOF-Confined Nanospaces: Tailored Architectures, Functions, and Applications, *Langmuir,* **36(36)**: 10657- 10673 (2020).

[28] Zhou H.-C., Kitagawa S., Metal–Organic, *Chem. Soc. Rev.,* **43**: 5415-5418 (2014).

[29] Liu L.L., Chen J., Zhang Y., Yu C.X., Du W., Sun X.Q., Lou Zhang J., Hu F.L., Mi Y., Ma L.F., Fabrication of Ultrathin Single-Layer 2D Metal-Organic Framework Nanosheets with Excellent Adsorption Performance via a Facile Exfoliation Approach, *J. Mater. Chem. A*, **9**: 546–555 (2021).

[30] Jiang D., Chen M., Wang H., Zeng G., Huang D., Cheng M., Liu Y., Xue W., Wang Z.W., The Application of Different Typological and Structural MOFs-Based Materials for the Dyes Adsorption, *Coord. Chem. Rev.,* **380**: 471-483 (2019).

[31] Haque, E., Khan N.A., Park J.H., Jhung S.H., Synthesis of a Metal-organic Framework Material, Iron Terephthalate, by Ultrasound, Microwave, and Conventional Electric Heating: A Kinetic Study, *Chem. Eur. J.*, **16(3)**: 1046-1052 (2010).

[32] Haque E., Jun J.W., Jhung S.H., Adsorptive Removal of Methyl Orange and Methylene Blue from Aqueous Solution with a Metal-Organic Framework Material, Iron Terephthalate (MOF-235), *J. Hazard. Mater.,* **185(1)**: 507-511 (2011).

[33] Tong M., Liu D., Yang Q., Devautourvinot S., Maurin G., Zhong C., Influence of Framework Metal Ions on the Dye Capture Behavior of MIL-100 (Fe, Cr) MOF Type Solids, *J. Mater. Chem. A*, **1(30)**: 8534–8537 (2013).

[34] Haque E., Lee J.E., Jang I.T., Hwang Y.K., Chang J.S., Jegal J., Jhung S.H., Adsorptive Removal of Methyl Orange from Aqueous Solution with Metal-Organic Frameworks, Porous Chromium-Benzenedicarboxylates, *J. Hazard. Mater.*, **181(1-3)**: 535-542 (2010).

[35] Haque E., Lo V., Minett A., Harris A. Church T., Dichotomous Adsorption Behaviour of Dyes on an Amino-Functionalised Metal–Organic Framework, Amino-MIL-101(Al), *J. Mater. Chem. A*, **2**: 193-203 (2014).

[36] Molavi H., Hakimian A., Shojaei A., Raeiszadeh M., Selective Dye Adsorption by Highly Water Stable Metal-Organic Framework: Long Term Stability Analysis in Aqueous Media, *Appl. Surf. Sci.*, **445**: 424-436 (2018).

[37] Carson C.G., Hardcastle K., Schwartz J., Liu X., Hoffmann C., Gerhardt R.A., Tannenbaum R., Synthesis and Structure Characterization of Copper Terephthalate Metal–Organic Frameworks, *Eur. J. Inorg. Chem.*, **16**: 2338-2343 (2009).

[38] Mohammadi N., Khani H., Gupta V.K., Amereh E., Agarwal S., Adsorption Process of Methyl Orange Dye onto Mesoporous Carbon Material–Kinetic and Thermodynamic Studies, *J. Colloid Interface Sci.,* **362(2)**: 457-462 (2011).

[39] Abbasi S., Ekrami-Kakhki M.-S., Tahari M., The Influence of ZnO Nanoparticles Amount on the Optimisation of Photo Degradation of Methyl Orange Using Decorated MWCNTs, *Prog. Ind. Ecol*., **13(1)**: 3-15 (2019).

[40] Roozban N., Abbasi S., Ghazizadeh M., The Experimental and Statistical Investigation of the Photo Degradation of Methyl Orange Using Modified MWCNTs with Different Amount of ZnO Nanoparticles, *J. Mater. Sci. Mater. Electron.*, **28(10)**: 7343–7352 (2017).

[41] Belbachir M., Bensaoula A., Composition and Method for Catalysis Using Bentonites, U.S. Patent No 6,274,527B1 (2006).

[42] Cherifi B.I., Belbachir M., Bennabi S., Green Polymerization of Vinyl Acetate Using Maghnite-Na^+, an Exchanged Montmorillonite Clay, as an Ecologic Catalyst, *Chem. Chem. Technol.,* **15(2)**: 183-190 (2021).

[43] Haoue S., Derdar H., Belbachir M., Harrane A., A New Green Catalyst for Synthesis of bis-Macromonomers of Polyethylene Glycol (PEG), *Chem. Chem. Technol.,* **14(4)**: 468 (2020).

[44] Derdar H., Meghabar R., Benachour M., Mitchell G.R., Bachari K., Belbachir M., Cherifi Z., Baghdadli M.C., Harrane A., Polymer-Clay Nanocomposites: Exfoliation and Intercalation of Organophilic Montmorillonite Nanofillers in Styrene–Limonene Copolymer, *Polym. Sci. – A,* **63**: 568-575 (2021).

[45] Embarek N., Sahli N., Ultrasound Assisted Synthesis of Polylimonene and Organomodified-clay Nanocomposites: A Structural, Morphological and Thermal Properties, *Bull. Chem. React. Eng. Catal.,* **15(3)**: 798-807 (2020).

[46] Derkaoui S., Belbachir M., A New Approach to Synthesis Methacrylic Monomers N-Alkylmethacrylamide Using an Ecologic and Friendly Catalyst Maghnite-H^+, *J. Fundam. Appl Sci.,* **11(1)**: 142-153 (2019).

[47] Bennabi S., Belbachir M., Synthesis and Characterization of New Organometallic Hybrid Material LCP-1 Based on MOF (Metal–Organic Framework) and Maghnite-H^+, a Protons Exchanged Montmorillonite Clay, as Catalytic Support, *J. Inorg. Organomet. Polym.,* **27**: 1787-1799 (2017).

[48] Chen Z., Zhang J., Fu J., Wang M., Wang X., Han R., Xu Q., Adsorption of Methylene Blue onto Poly(cyclotriphosphazene-co-4,4′-sulfonyldiphenol) Nanotubes: Kinetics, Isotherm and Thermodynamics Analysis, *J. Hazard. Mater.*, **273**: 263-271 (2014).

[49] Williams T.R., Handbook of Analytical Chemistry (Meites, Louis), *J. Chem. Educ.*, **40(10)**: 560 (1963).

[50] Qiu T., Zeng Y., Ye C., Tian H., Adsorption Thermodynamics and Kinetics of p-Xylene on Activated Carbon, *J. Chem. Eng. Data.*, **57(5)**: 1551-1556 (2012).

[51] Khan N.A., Hasan Z., Jhung S.H., Adsorptive removal of Hazardous Materials Using Metal-Organic Frameworks (MOFs): A Review, *J. Hazard. Mater.*, **244-245**: 444-456 (2013).

[52] Sarkar B., Xi Y., Megharaj M., Naidu R., Orange II Adsorption on Palygorskites Modified with Alkyl Trimethylammonium and Dialkyl Dimethylammonium Bromide — An Isothermal and Kinetic Study, *Appl. Clay Sci.,* **51(3)**: 370-374 (2011).

[53] Ai L., Zhang C., Meng L., Adsorption of Methyl Orange from Aqueous Solution on Hydrothermal Synthesized Mg-Al Layered Double Hydroxide, *J. Chem. Eng. Data,* **56(11)**: 4217-4225 (2011).

[54] Tsai F.-C., Xia Y., Ma N., Shi J.-J., Jiang T., Chiang T.-C., Zhang .Z-C., Tsen W.-C., Adsorptive Removal of Acid Orange 7 from Aqueous Solution with Metal–Organic Framework Material, Iron (III) Trimesate, *Desalin. Water Treat.,* **57(7)**: 3218-3226 (2014).

[55] Li H., Cao X., Zhang C., Yu Q., Zhao Z., Niu X., Sun X., Liu Y., Ma L., Li Z., Enhanced Adsorptive Removal of Anionic And Cationic Dyes from Single or Mixed Dye Solutions Using MOF PCN-222, *RSC Adv.,* **7**: 16273-16281 (2017).

[56] García E.R., Medina R.L., Lozano M.M., Pérez I.H., Valero M.J, Maubert Franco A.M., Adsorption of Azo-Dye Orange II from Aqueous Solutions Using a Metal-Organic Framework Material: Iron-Benzenetricarboxylate, *Materials,* **7(12)**: 8037-8057 (2014).

[57] Guo H., Lin F., Chen J., Li F., Weng W., Metal–Organic Framework MIL-125(Ti) for Efficient Adsorptive Removal of Rhodamine B from Aqueous Solution, *Appl. Organomet. Chem.,* **29(1)**: 12-19 (2015).

[58] Langmuir I., The Adsorption of Gases on Plane Surfaces of Glass, Mica and Platinium, *J. Am. Chem. Soc.,* **40(9)**: 1361-1403 (1918).

[59 Zhang F., Song W., Lan J., Effective Removal of Methyl Blue by Fine-Structured Strontium and Barium Phosphate Nanorods, *J. Lan, Appl. Surf. Sci.,* **326**: 195-203 (2015).

[60] Freundlich H.M.F., Over the Adsorption in Solution, *J. Phys. Chem.,* **57**: 385-471 (1906).

[61] Crini G., Peindy H.N., Gimbert F., Robert C., Removal of C.I. Basic Green 4 (Malachite Green) from Aqueous Solutions by Adsorption Using Cyclodextrin-Based Adsorbent: Kinetic and Equilibrium Studies, *Sep. Purif. Technol.,* **53(1)**: 97-110 (2007).

[62] Hao G., Li W., Wang S., Zhang S., Lu A., Tubular Structured Ordered Mesoporous Carbon as an Efficient Sorbent for the Removal of Dyes from Aqueous Solutions, *Carbon,* **48(12)**: 3330-3339 (2010).

[63] Lv S.-W., Liu J.-M., Ma H., Wang Z.-H., Li C.-H., Zhao N., Wang S., Simultaneous Adsorption of Methyl Orange and Methylene Blue from Aqueous Solution Using Amino Functionalized Zr-Based MOFs, *Micropor. Mesopor. Mat.*, **282**: 179-187 (2019).

[64] Lamari R., Benotmane B., Mostefa F., Removal of Methyl Orange from Aqueous Solution Using Zeolitic Imidazolate Framework-11: Adsorption Isotherms, Kinetics and Error Analysis, *Iran. J. Chem. Chem. Eng. (IJCCE)*, **41(6)**: 1985-1999 (2022).

[65] Rytwo G., Ruiz-Hitzky E., Enthalpies of Adsorption of Methylene Blue and Crystal Violet to Montmorillonite, *J. Therm. Anal. Calorim.,* **71**: 751-759 (2003).

[66] Song S., Ma Y., Shen H., Zhang M., Zhang Z., Removal and recycling of ppm Levels of Methylene Blue from an Aqueous Solution with Graphene Oxide, *RSC Adv.,* **5(35)**: 27922- 27932 (2015).

[67] Fernandes A.N., Almeida C.A.P, Debacher N.A., Isotherm and thermodynamic Data of Adsorption of Methylene Blue from Aqueous Solution onto Peat, *J. Mol. Struct.,* **982(1-3)**: 62-65 (2010).

[68] Zenasni M.A., Benfarhi S., Merlin A., Molina S., George B., Meroufel B., Adsorption of Cu(II) on Maghnite from Aqueous Solution: Effects of pH, Initial Concentration, Interaction Time and Temperature, *Nat. Sci.,* **10**: 856-868 (2012).

[69] Khan T.A., Khan E.A., Shahjahan, Removal of Basic Dyes from Aqueous Solution by Adsorption onto Binary Iron-Manganese Oxide Coated Kaolinite: Non-Linear Isotherm and Kinetics Modeling, *Appl. Clay Sci.,* **107**: 70-77 (2015).